Proceedings of International Conference on Heat Exchanger Fouling and Cleaning - 2011 (Peer-reviewed)
June 05 - 10, 2011, Crete Island, Greece
Editors: M.R. Malayeri, H. Müller-Steinhagen and A.P. Watkinson

Published online
www.heatexchanger-fouling.com

FOULING OF HEAT EXCHANGERS IN THE CONVECTION SECTION OF A THERMAL CRACKER

G.J. Heynderickx*, S.C.K. De Schepper and G.B. Marin

Laboratory for Chemical Technology, Ghent University
Krijgslaan 281 (S5), B-9000 Ghent, Belgium
geraldine.heynderickx@ugent.be

ABSTRACT

Fouling, due to coke formation in the heat exchanger tubes in the lower part of the convection section of a thermal cracker, used for pre-heating the hydrocarbon-steam reactor feed, is a rather recently observed phenomenon. It is most probably caused by a spray flow due to an incomplete evaporation of heavier crude oils in the heat exchangers in the upper part of the convection section. The fouling phenomenon is studied using a spray flow model, a droplet impact model and a coking model. The most vulnerable positions for fouling in the feed pre-heater tubes are determined. The spray flow droplet diameter is found to seriously influence the fouling positions in the heat exchanger tubes.

INTRODUCTION

Fouling due to coke formation in the reactor tubes suspended in the radiation section of a thermal cracker results in regular shut-downs of the thermal cracker to burn off the coke. This is a well-known, extensively studied phenomenon (Cai et al., 2002; Wauters and Marin, 2002). The radiation section is heated with floor burners and/or radiation wall burners. The energy remaining in the flue gas leaving the radiation section is further used in the convection section of the thermal cracker. In this section three basic heat exchangers with horizontal tubes are suspended. From the flue gas outlet (top of the section) to the flue gas inlet (bottom of the section), these heat exchangers are (1) the heat exchanger in which the liquid crude oil feed is (partially) evaporated, (2) the heat exchanger to produce over-heated steam and (3) the heat exchanger to pre-heat the hydrocarbon-steam mixture before feeding it to the reactor tubes. The crude oil is partially evaporated in the upper heat exchanger. The remaining liquid crude oil is evaporated in a nozzle, outside the convection section (not shown in Fig. 2a), where it is mixed with the over-heated steam coming from the middle heat exchanger. The use of a heavier crude oil however results in an incomplete evaporation of the liquid crude oil leaving the nozzle. The hydrocarbon-steam mixture that is fed to the lower heat exchanger still contains liquid (heavy) hydrocarbons. This observation is based on preliminary simulations of the convection section (De Schepper et al., 2009a,b), in which it was determined that the energy input in the convection section is insufficient to completely evaporate a heavy crude oil feed in the mixing nozzle where the output streams of the steam over-heater and the crude oil evaporator are mixed. Due to the presence of liquid hydrocarbons, the coke formation is observed to have extended from the reactor tubes in the radiation section to some of the heat exchangers tubes in the convection section, resulting in additional shut-downs of the thermal cracker. To prevent or reduce the fouling of the convection section heat exchanger tubes due to coke formation, the fouling process has been studied under the assumption that the non-evaporated crude oil in the hydrocarbon-steam mixture enters the feed pre-heater as a spray flow.

MODELING

Spray flow modeling

The spray flow crude oil droplets in the continuous vapor phase are modeled using the Eulerian-Lagrangian approach (Versteeg and Malalasekera, 1995; Ranade, 2002). The continuous vapor phase flow in the heat exchanger tubes is modeled using the Reynolds-Averaged Navier Stokes equations (RANS) (Versteeg and Malalasekera, 1995; Anderson, 2005), presented in Table 1 (Eqs. 1 to 3). The source terms in these equations keep track of the mass (S_M), momentum ($S_{F,i}$) and energy (S_E), lost or gained by a droplet. These source terms are defined in Table 2 (Eqs. 4 to 6). The averaged equations in Table 1 contain unclosed terms, the value of which is determined by introducing a so-called closure model: the turbulence model. The basic turbulence model is the k-ε model (Launders and Spalding, 1972). In the presented work, the Reynolds Stress Model (RSM) (Gibson and Launder, 1978) is used. This elaborated closure model, incorporated in the commercially available software package Fluent (2006), contains 6 conservation equations for the Reynolds stresses (Eq. 7 in Table 3) and 1 equation for the dissipation of turbulent energy. The RMS is the most appropriate model to study droplet trajectories in a continuous vapor flow as it accounts for streamline curvature, swirl flow, rotation and strain rate changes.

Force balances are used to determine the velocity components of a droplet in Cartesian coordinates. The main force contributions are the drag force and the gravity force. Next to the velocity, the position of the droplet is to be

determined as well (Eqs. 8 and 9 in Table 4). Finally, it is determined that, for the volume fractions of the droplets in the continuous vapor phase, lower than 10^{-4}, a two-way-coupling of the phases suffices (Ranade, 2002).

Table 1: Vapor phase Reynolds-Averaged Navier-Stokes equations

$$\frac{\partial}{\partial t}(\rho)+\sum_{i=1}^{3}\frac{\partial}{\partial x_i}\cdot(\rho\,\bar{u}_i)=S_M \quad (1)$$

$$\frac{\partial}{\partial t}(\rho\,\bar{u}_i)+\sum_{j=1}^{3}\frac{\partial}{\partial x_j}\cdot(\rho\bar{u}_i\bar{u}_j)= -\frac{\partial p}{\partial x_i}+\sum_{j=1}^{3}\frac{\partial}{\partial x_j}\left[\mu\left(\frac{\partial \bar{u}_i}{\partial x_j}+\frac{\partial \bar{u}_j}{\partial x_i}-\frac{2}{3}\delta_{ij}\sum_{l=1}^{3}\frac{\partial \bar{u}_l}{\partial x_l}\right)\right]+\sum_{j=1}^{3}\frac{\partial}{\partial x_j}\left(-\rho\overline{u_i'u_j'}\right)+S_{F,i} \quad (2)$$

$$\frac{\partial}{\partial t}(\rho E)+\sum_{j=1}^{3}\frac{\partial}{\partial x_j}\left(\rho E\,\bar{u}_j\right)=\sum_{i=1}^{3}\sum_{j=1}^{3}\left(\frac{\partial}{\partial x_j}\left(\tau_{ij}-\rho\overline{u_i'u_j'}\right)\bar{u}_i\right)-\sum_{j=1}^{3}\frac{\partial}{\partial x_j}q_j+S_E \quad (3)$$

Table 2: Source terms of continuous vapor phase RANS equations

$$S_M=\frac{\Delta m_p}{m_{p,0}}\dot{m}_{p,0} \quad (4)$$

$$S_{F,i}=\left(\frac{18\,\mu\,C_D Re_{d,i}}{24\,\rho_p d_p^2}\left(u_{p,i}-u_i\right)+F_{other}\right)\dot{m}_p\,\Delta t \quad (5)$$

$$S_E=\left[\frac{\Delta m_p}{m_{p,0}}c_p\,\Delta T_p+\frac{\Delta m_p}{m_{p,0}}\left(-h_{fg}+\int_{T_{ref}}^{T_p}c_p dT\right)\right]\dot{m}_{p,0} \quad (6)$$

Table 3: Transport equations for the Reynolds stresses

$$\underbrace{\frac{\partial}{\partial t}\left(\rho\overline{u_i'u_j'}\right)}_{\text{Local time derivative}}+\underbrace{\frac{\partial}{\partial x_k}\left(\rho u_k\overline{u_i'u_j'}\right)}_{C_{ij}\equiv\text{Convection}} =\underbrace{-\frac{\partial}{\partial x_k}\left[\rho\overline{u_i'u_j'u_k'}+\overline{p\left(\delta_{kj}u_i'+\delta_{ik}u_j'\right)}\right]}_{D_{T,ij}\equiv\text{Turbulent diffusion}}+\underbrace{\frac{\partial}{\partial x_k}\left[\mu\frac{\partial}{\partial x_k}\left(\overline{u_i'u_j'}\right)\right]}_{D_{L,ij}\equiv\text{Molecular diffusion}}$$

$$\underbrace{-\rho\left(\overline{u_i'u_k'}\frac{\partial u_j'}{\partial x_k}+\overline{u_j'u_k'}\frac{\partial u_i'}{\partial x_k}\right)}_{P_{ij}\equiv\text{Stress production}}\underbrace{-\rho\beta\left(g_i\overline{u_j'\theta}+g_j\overline{u_i'\theta}\right)}_{G_{ij}\equiv\text{Buoyancy production}}$$

$$\underbrace{+\overline{p\left(\frac{\partial u_i'}{\partial x_k}+\frac{\partial u_j'}{\partial x_i}\right)}}_{\varphi_{ij}\equiv\text{Pressure strain}}\underbrace{-2\mu\overline{\frac{\partial u_i'}{\partial x_k}\frac{\partial u_j'}{\partial x_k}}}_{\varepsilon_{ij}\equiv\text{Dissipation}} \quad (7)$$

Table 4: Velocity and position of droplet in i-direction

$$\frac{du_{p,i}}{dt}=\frac{18\mu}{\rho_p d_p^2}\cdot\frac{C_D Re_{d,i}}{24}\cdot\left(u_i-u_{p,i}\right)+\frac{g_i\left(\rho_p-\rho\right)}{\rho_p}+F_i \quad (8)$$

$$\frac{dx_{p,i}}{dt}=u_{p,i} \quad (9)$$

Droplet Impact Behavior Modeling

Droplets impinging on the heat exchanger tube wall are expected to be the origin of coke formation. The droplet impact model presented by Wachters and Westerling, 1966, has been confirmed by Mundo et al., 1995, and Gavaises et al., 1996. The model describes a situation in which a droplet that impinges on a tube wall either sticks, rebounds back into the continuous flow or splashes. In the latter case, a fraction of the droplet sticks to the surface, while the remaining fraction breaks up into smaller droplets that rebound back into the continuous flow. The higher the droplet impact energy on the wall, the lower the fraction of the droplet that sticks to the wall. The droplet impact behavior and the decision chart to determine this impact behavior are presented in Fig. 1 (De Schepper, 2008). This decision chart, used in the presented work to determine the droplet behavior, depends on the Weber number, comparing the fluid's inertia to its surface tension (Wachters and Westerling, 1966) and on the heat exchanger tube wall temperature as compared to the boiling temperature of the liquid hydrocarbons (Mundo et al., 1995). The stick behavior is discussed in detail by Bai and Gosman, 1995; the rebound behavior by Kandlikar and Steinke, 2002. A

simplified model for the splashing behavior, used in the presented work, is developed by Grover and Assanis, 2001.

Coke Formation Modeling

The cracking reactions in the reactor tubes in the radiation section of a thermal cracker are inherently linked to coke formation. The coking reactions depend, amongst other, on the tube wall temperature. Coking models have been developed for coke formation in the reactor tubes in the radiation section of the thermal cracker (Cai et al., 2002; Wauters and Marin, 2002). However, these models are assumed to be invalid for the present study as the temperature of the heat exchanger tube walls in the convection section of the thermal cracker is considerably lower than the reactor tube wall temperatures in the radiation section of the thermal cracker, and thus not within the temperature range for which the available cracking models were developed.

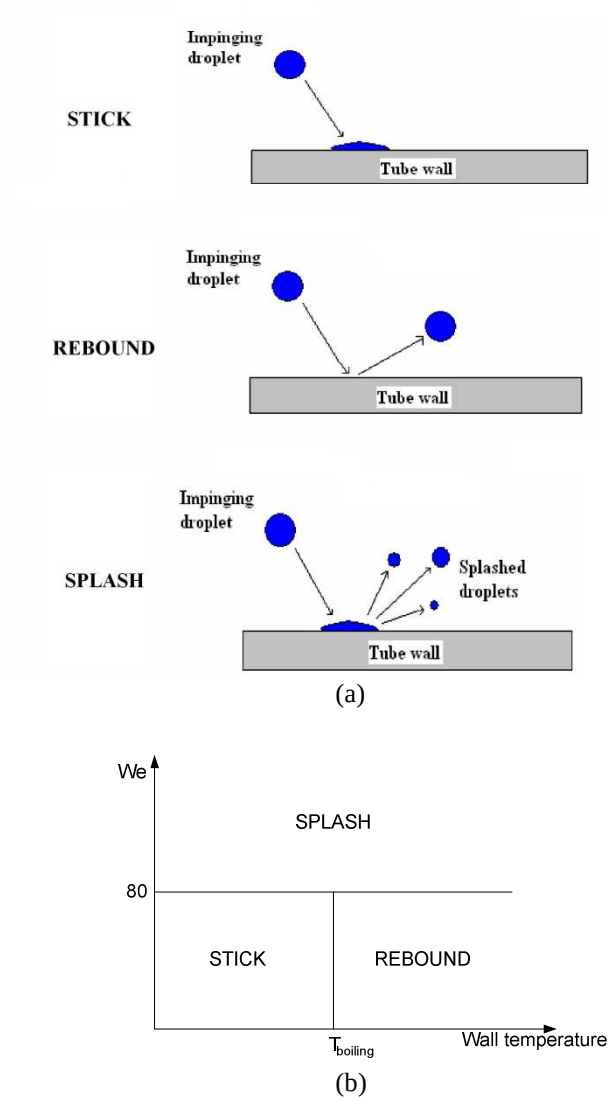

Fig. 1: Droplet impact behavior (a) with decision chart (b) (De Schepper, 2008)

Simplified coking rate mechanisms and kinetics are found in literature, ranging from one-step (Chin et Lefebvre, 1995) over two- and three-step mechanisms (Giovanetti and Szetela, 1986; Krazinski et al., 1992) to a nine-step mechanism (Katta et al., 1993). For the presented study, one step from the nine-step mechanism presented by Katta et al., 1993, is selected, transforming a coke precursor P into a coke deposit on the heat exchanger tube skin. The corresponding kinetics are calculated from:

$$r = A\, e^{\frac{-E_a}{RT}} [P] \qquad (10)$$

The values of the kinetic parameters (A=260m/s and E_a=71.18kJ/mol) were determined by Ervin and Williams, 1996, based on experimental data in the temperature range of 298 to 546K, a temperature range corresponding to the heat exchanger tube wall temperatures where coke formation is observed. Coke precursors P have to be selected. From the research in the thermal cracker reactor tubes in the radiation section (Kopinke et al., 1993a,b), it is well-known that aromatic components have a high tendency to form coke. For the heavy crude oil feed (over 20 wt% over n-paraffines-15) (De Schepper, 2008), aromatics are selected as coke precursors.

SOLUTION TECHNIQUES

Simulations are based on a second-order calculation scheme (Versteeg and Malalasekera, 1995) for the RANS equations and the RSM. The PISO algorithm (Issa, 1986) is applied to couple pressure and velocity. As it is important for the presented study to correctly capture the near-wall behavior of the flow, especially of the droplet, a grid with three layers of small grid cells (of the order of magnitude of the droplets) is constructed near the heat exchanger tube walls. The 3-D-computational domain of mixture over-heater 1 (see Fig. 2a) is divided into 1,764,315 hexahedral cells.

CONVECTION SECTION

A cross section of the convection section of the thermal cracker is presented in Fig. 2a, together with the definition of zones and sub-zones on the simulated heat exchanger tubes (Fig. 2b). The tubes of mixture over-heater 1 have a diameter of 0.0779m and a one-pass length of 11.3m.

For a detailed overview and discussion of the convection section geometry and operating conditions, reference is made to De Schepper et al., 2009a,b. Different tube rows are defined, each containing a number of vertical U-bends. By paying attention to the way the tubes are shaded in Fig. 2a, one can follow the flow direction of the evaporating liquid crude oil from top to bottom in the convection section. Simulations (De Schepper et al., 2009a) have shown that less than 30wt% of a heavy crude oil is evaporated in the upper heat exchanger. This liquid/vapor flow is mixed with the over-heated steam in a mixing nozzle situated outside the convection section. First simulations (De Schepper et al., 2009b) have shown that the mixing does not suffice to completely evaporate the heavy crude oil. A spray flow is supposed to leave the mixing nozzle and enter mixture over-heater 1. In tube rows 1.1 to 1.3 (see Fig. 2a) fouling by coke formation is observed.

RESULTS

The behavior of droplets with different diameters in a tube of the mixture over-heater 1, making three passes in the convection section, as seen in Fig. 2a, has been studied. The studied droplet diameters are 0.1; 1; 10; 50 and 100 micron, the liquid crude oil (De Schepper, 2008; De Schepper et al., 2009a) is calculated to have a density of 718 kg/m^3, a boiling temperature of 622K and a surface tension of 0.018N/m. For all droplet diameters, 6000 droplets have been injected in the studied tube, implying that the total amount of non-evaporated heavy crude oil injected in the heat exchanger tube rises with rising droplet diameter. The weight fraction of the injected droplets that is deposited in the tube entrance zone 2 (see Fig. 2b) for the different droplet diameters is presented in Fig. 3. The deposit of coke mass for the different droplet diameters is presented in Fig. 4a-e. For the 1 micron droplets, the dispersion of the deposited cokes over the tube circumference (see Fig. 2b) is presented as well. Finally, Fig. 5a-c presents the coking rates, calculated based on Eq. 10.

DISCUSSION

Based on Fig. 4a-e, it can be determined which are the critical zones for coke formation in the tubes. Whatever the droplet diameter, the most vulnerable zones are the zones following the inlet bend, due to a frequent droplet impact. A typical tube wall temperature in the bend is 450K , well below the boiling point temperature of 622K. For the smaller droplets (low Weber number) an impact results in a 'STICK' as seen on the decision chart (Fig. 1b). For the larger droplets (high Weber number) an impact results in a 'SPLASH'. In the simplified splashing model of Grover and Assanis, 2001, a fraction of the splashing droplet will always stick to the surface. The first of the two U-bends of the tube is a critical position as well. The droplet cannot follow the vapor flow direction in the U-bend and impinges on the wall. Nevertheless, the distribution of the coke mass over the entire tube length clearly differs depending on the droplet diameter. For the smallest droplets (Fig. 4a-b), coke is deposited along the entire tube length, that is in the three tube passes. This is to be expected as smaller droplets can more easily follow the vapor flow direction and thus reach tube pass 3. Their impact is more 'coincidental' and due to molecular diffusion and flow turbulence. For the larger droplets (Fig. 4d-e), coke formation is observed in the first tube pass only. Due to their dimension these droplets are not capable of following the vapor flow direction, as they have a higher inertia than the smaller droplets. The droplets already impinge and partially stick to the tube wall in the tube entrance zone. Upon impact, these large droplets partially stick to the tube surface and partially splash into smaller droplets. Due to consecutive splashing, small droplets are formed out of these large droplets. Nevertheless, only a small amount of liquid remains in the

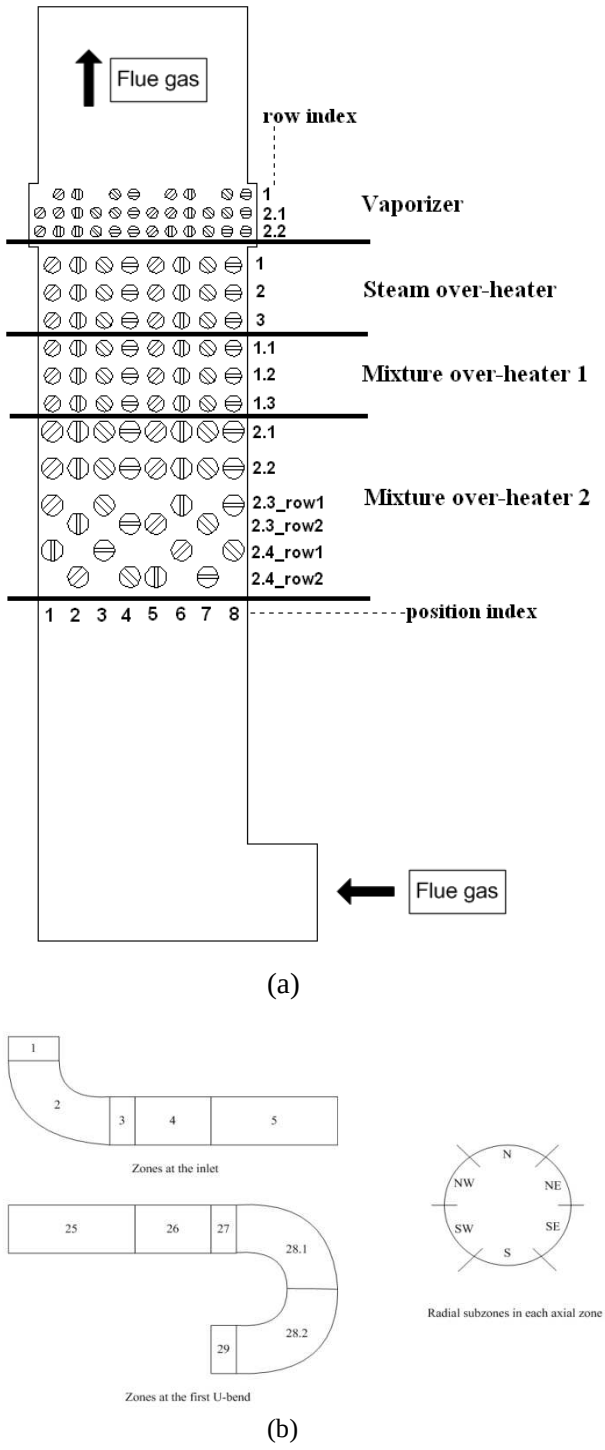

Fig. 2: Cross-section (a) and tube zoning (b) of the convection section (De Schepper et al., 2009b)

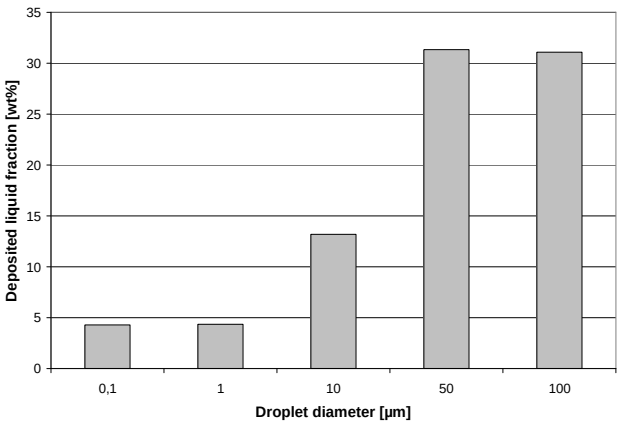

Fig. 3: Fraction of droplets deposited in the tube entrance zone 2 (see Fig. 2b)

vapor during the consecutive splashing. It is calculated that for the larger droplets already over 30 wt% of the injected liquid is deposited in the tube entrance zone 2. For the smaller droplets this value is less than 5 wt%. The latter is shown in Fig. 3. Remark that the value of deposited liquid for the 50 micron droplets is larger than the value for the 100 micron droplets. The latter is due to the higher impact energy of the 100 micron droplets, resulting in a lower fraction of the liquid sticking to the tube wall. For the larger droplets (Fig.4d-e), all liquid is already deposited before entering tube pass 3; while the liquid deposition in tube pass 2 is extremely low and limited to the tube zones following the U-bend. As a consequence, nearly no coke is observed in tube pass 2, while there is no coke observed in tube pass 3. Accounting for the high total liquid injection, a relatively thick layer of coke will be formed out of the larger droplets in tube pass 1.

Fig. 4b gives an overview of the coke deposit along the tube circumference as well. As expected, accounting for the entrance direction of the liquid spray and accounting for gravity, the deposited coke mass is higher on the 'S' positions (see Fig. 2b).

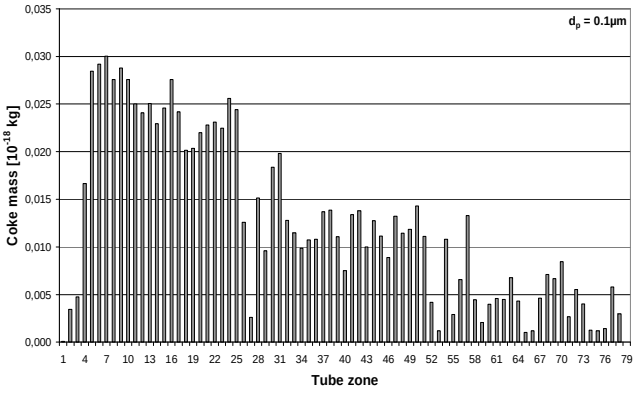

(a)

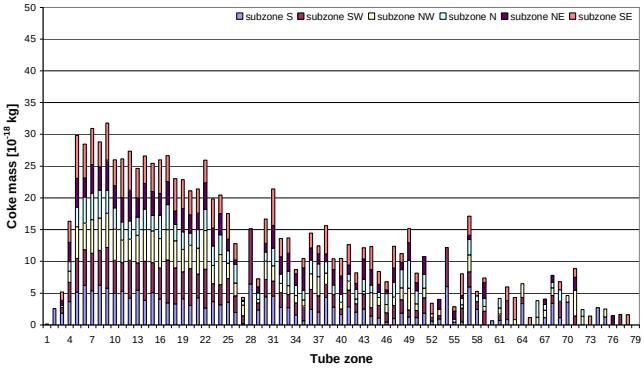

(b)

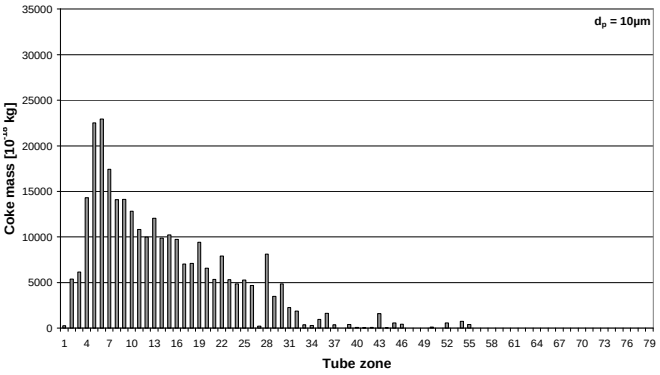

(c)

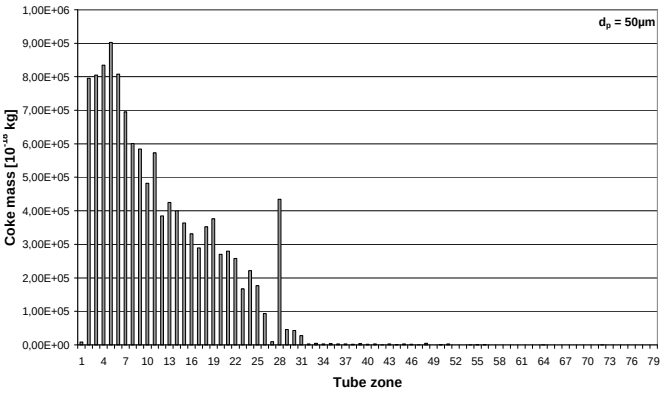

(d)

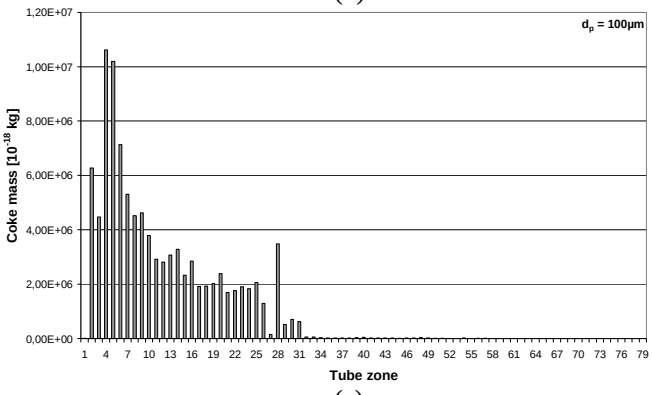

(e)

Fig. 4a-e: Mass of coke formed in (sub) zones of a three pass heat exchanger tube for the injected droplets.

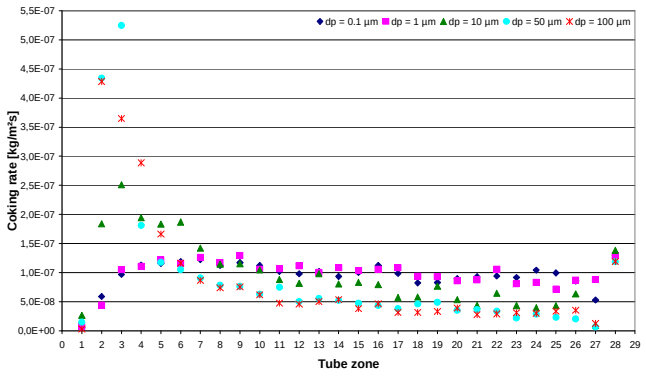

(a)

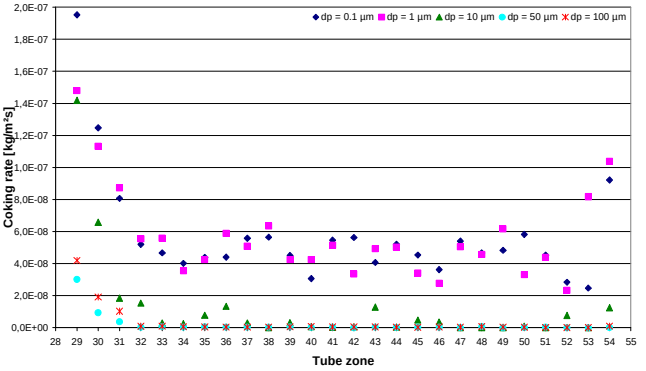

(b)

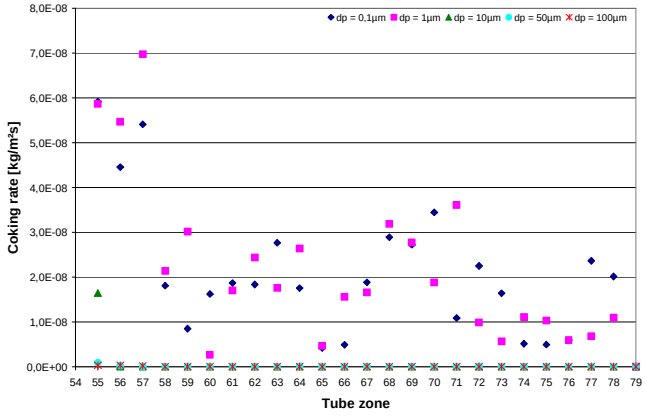

(c)

Fig. 5a-c: Coking rate in the three tube passes for different diameter droplets (Eq. 10)

Finally, Fig. 5a-c presents the calculated coking rates, using Eq. 10, along the complete tube length for the different droplet diameters. Indeed, for all droplet diameters, the coking rate differs from zero in the first tube pass (Fig. 5a). For the second tube pass (Fig. 5b) the coke formation for the larger droplets is found to be zero. For the 10 µm droplets, the coking rate slowly drops to a value of zero in the second tube pass. In the final tube pass (Fig. 5c) only the two smallest droplets are calculated to have a (low) coking rate. The latter calculations correspond to the results presented in Figure 4a-e.

CONCLUSIONS

The tube zones in the convection section heat exchangers vulnerable for fouling due to coke formation are identified, using a spray flow model. The latter will help to optimize the coupled operation of both the radiation and the convection section of a thermal cracker. This optimization will result in limiting the number of shut-downs of a thermal cracker and thus the economic losses. It is found that for a spray of small droplets entering the feed pre-heater in the convection section, drag force overcomes gravity and coke deposition is observed along the entire tube length. For a spray of larger droplets, inertia overcomes drag and most of the fouling is observed in the first tube pass, near the tube entrance and in the first U-bend of the three-pass tube. The results are confirmed by the calculated coking rates, using a coking model, for the different droplet diameters in the different tube passes.

ACKNOWLEDGMENT

The CFD research in thermal cracking (G.J. Heynderickx) is supported by the Fonds voor Wetenschappelijk Onderzoek-Vlaanderen (FWO-Vlaanderen) (project G.0022.09).
Sandra De Schepper would like to thank SABIC Europe for supporting this research study.

NOMENCLATURE

A	pre-exponential factor , m/s
c_p	heat capacity, J/kg K
C_D	drag coefficient, -
d	diameter, m
E	total energy per unit mass, J/kg
E_a	activation energy, kJ/mol
F	external body forces, kg/m²s²
g	gravitational acceleration, 9.81 m/s²
h_{fg}	latent heat, J/kg
m	mass, kg
$\dot{m}$	mass flow rate, kg/s
p	pressure, Pa
$[P]$	mass concentration of the coke precursor, kg/m³
q	conductive heat flux, J/m²s
Re_d	Reynolds number based on droplet diameter and relative velocity = $\frac{\rho d_p \lvert u_p - u \rvert}{\mu}$, -
r	reaction rate, kg/m²s
S_E	source term in the energy equation, J/m³s
S_F	source term in the momentum conservation equation , kg/m²s²
S_M	source term in the mass conservation equation, kg/m³s
T	temperature, K
$T_{boiling}$	boiling temperature (Fig. 1), K
t	time, s
u	velocity of the continuous vapor phase, m/s
u_p	droplet velocity, m/s
$\bar{u}$	Reynolds average of u, m/s
u'	Reynolds fluctuation of u, m/s
u_k	velocity of phase k, m/s
u_n	droplet velocity component normal to the

tube wall surface, m/s

We Weber number = $\frac{\rho_p u_n^2 d_p}{\sigma}$, -

x Cartesian coordinate, m

y Cartesian coordinate, m

z Cartesian coordinate, m

Greek symbols

β thermal expansion coefficient, -

δ_{ij} Kronecker function, -

μ dynamic viscosity, Pa·s

ρ density, kg/m³

σ vapor-liquid surface tension, N/m

τ viscous stress, kg/ms²

Subscripts

i i-direction

j j-direction

k phase k

l l-direction

n normal

o original

p droplet

REFERENCES

J.D. Anderson, 2005, *Computational Fluid Dynamics: The Basics with Applications*. McGraw-Hill, New York.

C. Bai; A.D. Gosman, 1995, Development of methodology for spray impingement simulation. SAE Technical Paper 950283.

H. Cai; A. Krzywicki.; M.C. Oballa, 2002, Coke formation in steam crackers for ethylene production, *Chem. Eng. Process*, Vol. 41, p.199.

J. Chin; A. Lefebvre, 1995, Influence of flow conditions on deposits from heated hydrocarbon fuels, Presented at the International Gas Turbine and Aeroengine Congress and Exposition, Cologne, Germany, *ASME paper* 92-GT-114

S.C.K. De Schepper, 2008, Simulation of the convection section of a steam cracker, *Doctoral thesis*, Ghent University, Belgium

S.C.K. De Schepper; G.J. Heynderickx; G.B. Marin, 2009a, Modeling the evaporation of a hydrocarbon feedstock in the convection section of a steam cracker, *Comp. and Chem. Eng.*, Vol. 33, p. 122.

S.C.K. De Schepper; G.J. Heynderickx; G.B. Marin, 2009b, Coupled Simulation of the Flue Gas and Process Gas Side of a Steam Cracker Convection Section, *AIChE Journal*, Vol. 55, p. 2773.

J. Ervin, T. Williams,1996, Global kinetic modeling of aviation fuel fouling in cooled regions in a flowing system, *Ind. Eng. Chem. Res.*, Vol. 35, p. 4028.

Fluent Inc., 2006 , *Fluent 6.3 User's Guide*, Lebanon, USA.

M. Gavaises; A. Theodorakakos; G. Bergeles, 1996, Modeling wall impaction of diesel sprays, *Int. J. Heat and Fluid Flow*, Vol. 17, p.130.

M.M. Gibson; B.E. Launder, 1978, Ground Effects on Pressure Fluctuations in the Atmospheric Boundary Layer, *J. Fluid Mech.*, Vol. 86, p. 491.

A. Giovanetti; E. Szetela, 1986, Long term deposit formation in aviation turbine fuel at elevated temperature, In 24th Aerospace Sciences Meeting, Reno, NV.*AIAA Paper* 86-0525

R.O. Grover; D.N. Assanis, 2001, A Spray Wall Impingement Model Based Upon Conservation Principles, Fifth International Symposium on Diagnostics and Modeling of Combustion in Internal Combustion Engines, p. 551.

R.I. Issa, 1986, Solution of the Implicitly Discretized Fluid Flow Equations by Operator Splitting, *J. Comput. Phys*,, Vol. 62, p. 40.

S.G. Kandlikar.; M.E. Steinke, 2002, Contact angles and interface behavior during rapid evaporation of a liquid on a heated surface, *Int. J. Heat and Mass Transfer*, Vol. 45.

V.Katta; E. Jones; W. Roquemore, 1993, Development of global chemistry model for jet-fuel thermal stability based on observations from static and flowing experiments, AGARD-CP-536, Paper no. 19.

F. Kopinke; G. Zimmermann; G. Reyniers; G. Froment, 1993a, Relative rates of coke formation from hydrocarbons in steam cracking of naphtha, 2. Paraffins, naphtenes, mono-, di-, and cycloolefins, and acetylenes, *Ind. Eng. Chem. Res.*, Vol. 32, p. 56.

F. Kopinke; G. Zimmermann; G. Reyniers; G. Froment, 1993b, Relative rates of coke formation from hydrocarbons in steam cracking of naphtha. 3. Aromatic hydrocarbons, *Ind. Eng. Chem. Res.*, Vol. 32, p. 2620.

J. Krazinski; S. Vanka; J. Pearce; W. Roquemore, 1992, A computational fluid dynamics and chemistry model for jet fuel thermal stability, *Journal of Engineering for Gas Turbines and Power*, Vol. 114, p. 104.

B.E. Launder; D.B. Spalding, 1972, *Lectures in Mathematical Models of Turbulence*. Academic Press, London, England.

C. Mundo; M. Sommerfeld; C. Tropea, 1995, Droplet-Wall Collisions: Experimental Studies of the Deformation and Breakup Process, *Int. J. Multiphase Flow*, Vol. 21, p. 151.

V.V. Ranade, 2002, *Computational Flow Modeling for Chemical Engineering*, Vol.5, Academic Press, San Diego, California.

H.K. Versteeg; W. Malalasekera, 1995, *An introduction to Computational Fluid Dynamics, The Finite Volume Method*, Longman Scientific and Technical, Harlow, Essex, UK.

H.J. Wachters; N.A.J. Westerling, 1966, The heat transfer from a hot wall to impinging water drops in a spheroidal state, *Chem. Eng. Sci.*, Vol. 21, p. 1047.

S. Wauters; G.B. Marin, 2002, Kinetic modeling of coke formation during steam cracking, *Ind. Eng. Chem. Res.*, Vol. 41, p. 2379.